CHEMISTRY OF MATERIALS
Article

Chem. Mater. **2010,** *22,* 2287–2296 2287
DOI:10.1021/cm903166f

Directed Growth of 1D Assemblies of Perylene Diimide from a Conjugated Polymer

Zhongyuan Zhou, Jaclyn L. Brusso, and Steven Holdcroft*

Department of Chemistry, Simon Fraser University, Burnaby, British Columbia V5A 1S6, Canada

Received October 14, 2009. Revised Manuscript Received January 15, 2010

The templated growth of 1D assemblies of perylene diimides (PDI) formed within a conjugated polymer is described. The formation of this unique morphology is accomplished through the synthesis of a PDI-functionalized conjugated polymer and its solution casting in the presence of PDI. The strategy is demonstrated with poly(3-hexylthiophene) (P3HT), partially functionalized at the 4-position with *N*-(1-hexylheptyl)-*N*′-(12-carboxylicdodecyl)perylene-3,4,9,10-tetracarboxylbisimide (PP3HT). The 1D assemblies of PDI embedded in the optoelectronically active polymer are hundreds of nanometers wide, 10−20 nm thick, several micrometers in length, and run parallel to the surface of the substrate. Surrounding the 1D structures is a heterogeneous PP3HT-PDI blend, comprising PP3HT domains less than 10 nm in size. Excitation energy in thin film blends of PP3HT:PDI is quenched to a much greater extent than simple molecular blends of P3HT and PDI. These systems represent structures of multiple hierarchy, wherein nanosized domains of a π-conjugated polymer and an n-type material are in intimate contact and which encapsulate 1D assemblies of nanocrystallites that run parallel to the films surface. They offer an alternative route for the fabrication of innovative supramolecular structures for optoelectronic applications.

Introduction

π-Conjugated organic materials have attracted considerable attention over the past three decades on account of their special properties, which include electronic conductivity, electroluminescence, and light-harvesting. The use of these materials in thin-film electronics is a driving force behind the development of new and modified π-conjugated systems; however, a greater understanding of structure−property relationships is vital to reaching this goal. Recently, research has focused on the formation of nanosized structures by molecular self-assembly of tailored, supramolecular building blocks. Through noncovalent interactions (e.g., hydrophobic, electrostatic, $\pi-\pi$ stacking, hydrogen bonding)[1−6] a variety of supramolecular architectures (e.g., spherical micelles, vesicles, fibers, supramolecular helices, nanoribbons, and nanotubes)[7−13] have been fabricated. Although research in this field has led to a greater understanding of the requirements for supramolecular engineering,[1] the creation of supramolecular architectures with well-defined shapes, structure, and functions continues to be a significant challenge.

Among the many types of supramolecular building blocks, the most widely studied systems are rod−coil oligomers and polymers consisting of rigid, rodlike, and flexible, coil-like blocks within the same molecular backbone. These materials are excellent candidates for creating supramolecular structures because of mutual repulsion of the dissimilar blocks that result in microphase segregation of rod and coil segments into ordered periodic arrays.[14] Recently, triblock copolymers which can exist as either coil−rod−coil or rod−rod−rod conformations were reported by Mezzenga et al. The transition between configurations, triggered either thermally or via variation in solvent composition, result in lamellar ordering or clustering, respectively.[15] Alternatively, ordered structures may be obtained from crystalline−crystalline diblock copolymers. For example, regioregular poly(3-butylthiophene)-*b*-poly(3-octylthiophene) in various compositions was found to self-assemble into crystalline nanowires from solution and, from the melt phase, to microphase-separate into two distinct crystalline

*Corresponding author.

(1) Hoeben, F. J. M.; Jonkheijm, P.; Meijer, E. W.; Schenning, A. *Chem. Rev.* **2005**, *105*, 1491–1546.
(2) Ligthart, G.; Ohkawa, H.; Sijbesma, R. P.; Meijer, E. W. *J. Am. Chem. Soc.* **2005**, *127*, 810–811.
(3) Berl, V.; Schmutz, M.; Krische, M. J.; Khoury, R. G.; Lehn, J. M. *Chem.—Eur. J.* **2002**, *8*, 1227–1244.
(4) Faul, C. F. J.; Antonietti, M. *Adv. Mater.* **2003**, *15*, 673–683.
(5) Wong, G. C. L.; Tang, J. X.; Lin, A.; Li, Y. L.; Janmey, P. A.; Safinya, C. R. *Science* **2000**, *288*, 2035–2039.
(6) Lehn, J. M. *Science* **2002**, *295*, 2400–2403.
(7) Ryu, J. H.; Hong, D. J.; Lee, M. *Chem. Commun.* **2008**, 1043–1054.
(8) Kim, H. J.; Lim, Y. B.; Lee, M. *J. Polym. Sci., Part A: Polym. Chem.* **2008**, *46*, 1925–1935.
(9) Fuhrhop, A. H.; Wang, T. Y. *Chem. Rev.* **2004**, *104*, 2901–2937.
(10) Shimizu, T.; Masuda, M.; Minamikawa, H. *Chem. Rev.* **2005**, *105*, 1401–1443.
(11) Palmer, L. C.; Stupp, S. I. *Acc. Chem. Res.* **2008**, *41*, 1674–1684.
(12) Antonietti, M.; Forster, S. *Adv. Mater.* **2003**, *15*, 1323–1333.
(13) Lazzari, M.; Lopez-Quintela, M. A. *Adv. Mater.* **2003**, *15*, 1583–1594.
(14) Lee, M.; Yoo, Y. S. *J. Mater. Chem.* **2002**, *12*, 2161–2168.
(15) Rubatat, L.; Kong, X. X.; Jenekhe, S. A.; Ruokolainen, J.; Hojeij, M.; Mezzenga, R. *Macromolecules* **2008**, *41*, 1846–1852.

Published on Web 02/16/2010

domains possessing a lamellar structure.[16] Sary et al. have also reported on blends of a rod-type homopolymer with rod−coil block copolymers in which long-range lamellar clusters percolate throughout the entire sample. It was noted that such ordering was not observed upon blending the rod-type polymer with the coil-type homopolymer, thus attributing the ordered lamallar clusters to $\pi-\pi$ interactions between rod segments.[17]

Dendritic materials have also garnered a great deal of attention in the drive to develop ordered structures for optoelectronic applications.[18] For example, Stupp et al. have incorporated dendritic blocks into rod−coil materials at the end of the rod segment (e.g., **1** in Chart 1). The relative size of the dendron with respect to the rod−coil segment significantly influences the packing, either promoting or inhibiting long-range molecular assembly.[19] A number of one-dimensional nanostructures based on flat and helical nanoribbons have been assembled using dendron−rod−coil molecules. Furthermore, introduction of functionality onto the dendritic block in the form of hydroxyl groups or electronically conductive substitutents provides nanoassemblies with potential applications as biomaterials, nonlinear optics and nanowires.[11] Similarly, Lee et al. have demonstrated that 1D cylindrical assemblies may be formed from wedge-coil molecules. As opposed to dendron−rod−coil systems, these materials possess tunable properties triggered by external stimuli such as solvent polarity.[20] For example, as the solvent polarity is changed from water to hexane, the self-assembled nanofibers of molecule **2** become inverted resulting in conversion of highly flexible, coil-like to stiff, rodlike cylinders. Such structural inversions may be utilized in applications such as encapsulation and smart surfaces.[20] Besides solvent effects, enhanced $\pi-\pi$ interactions significantly influence the self-assembly of 1D nanostructures as is observed with **3**, in which aggregation into twisted helical ribbons with regular periodicity occurs.[21]

Attachment of bulky dendrons to both ends of a rigid rod, such as the dumbbell molecule **4**, promotes $\pi-\pi$ stacking of the aromatic groups. In this case, mutual rotation to relieve steric hindrance due to the bulky dendrons results in aggregation into regular helical arrangements.[7] Furthermore, transformation of the helical strands into nanocages can be achieved through addition of aromatic guest molecules. The authors attribute this to intercalation of the guest molecule between the rod segments via $\pi-\pi$ interactions, thus partially relieving steric repulsion between the bulky dendrons and illustrating the impact $\pi-\pi$ interactions can impart on the aggregation of molecules.[7] Similarly, the shape-dependent organization of perylene diimides (PDI) has been reported by Würthner et al. in which the wedge-shaped PDI **5** assembles into small micellar aggregates and the dumbbell-shaped PDI **6** forms nanorod aggregates.[22] Interestingly, the authors found that mixtures of wedge-shaped and dumbbell-shaped PDIs formed hollow vesicles due to coassembly. In other words, alternation between a bulky symmetric PDI with an unsymmetric wedge-shaped PDI decreases the curvature with respect to the micelle formed by **5** alone and increases the curvature with respect to the nanorods of **6**, and thus vesicles are formed over micelles or nanorods. Collectively, these structural effects on morphology provide a guideline for the rational design of particular morphologies.[22]

The planar π-conjugated framework of PDI molecules coupled with their inherent n-type semiconductor characteristics and high thermal and photostability make these ideal candidates for supramolecular self-assembly into 1D nanoarchitectures through strong $\pi-\pi$ interactions. Their potential use in device applications provides the impetus for optimization of the molecular structure to achieve shape-defined 1D assemblies with desired optoelectronic properties. Thus, fabrication of 1D nanostructures, based on PDI, with controllable size and morphology has been investigated by Zang and co-workers. Their research has demonstrated that assembly of PDI into 1D structures requires cofacial $\pi-\pi$ stacking between molecular skeletons to predominate over lateral association caused by the hydrophobic interaction among the side chain substituents.[23] Through a variety of techniques (e.g., phase transfer, vapor diffusion, seeded growth) Zang et al. have been successful at generating nanobelts, nanowires, and nanofibers from PDI systems that would otherwise form bulky aggregates.[23] Under similar conditions, other research groups have also isolated PDI nanowires and nanofibers by phase transfer and solvent-vapor annealing, respectively.[24,25] Recently, a new class of polymeric multichromophoric arrays in which PDI molecules are linked to a polymeric backbone via small peptidic spacers has been reported.[26] In these perylene polyisocyanides, the PDI moieties have rotational and translational freedom to allow for rearrangement on the molecular scale; however, on a larger scale, they form highly defined arrays along the polymer backbone through $\pi-\pi$ stacking. This "locking in" of the PDI molecules, essentially forming π-stacks along the polymer backbone, confers electronic and optical function to the architecture.[27,28]

(16) Wu, P. T.; Ren, G. Q.; Li, C. X.; Mezzenga, R.; Jenekhe, S. A. *Macromolecules* **2009**, *42*, 2317–2320.
(17) Sary, N.; Mezzenga, R.; Brochon, C.; Hadziioannou, G.; Ruokolainen, J. *Macromolecules* **2007**, *40*, 3277–3286.
(18) Lo, S. C.; Burn, P. L. *Chem. Rev.* **2007**, *107*, 1097–1116.
(19) Palmer, L. C.; Velichko, Y. S.; de la Cruz, M. O.; Stupp, S. I. *Philos. Trans. R. Soc., Ser. A* **2007**, *365*, 1417–1433.
(20) Kim, J. K.; Lee, E.; Lee, M. *Angew. Chem., Int. Ed.* **2006**, *45*, 7195–7198.
(21) Lee, E.; Huang, Z.; Ryu, J. H.; Lee, M. *Chem—Eur. J.* **2008**, *14*, 6957–6966.
(22) Zhang, X.; Chen, Z. J.; Wurthner, F. *J. Am. Chem. Soc.* **2007**, *129*, 4886–4887.
(23) Zang, L.; Che, Y. K.; Moore, J. S. *Acc. Chem. Res.* **2008**, *41*, 1596–1608.
(24) Briseno, A. L.; Mannsfeld, S. C. B.; Reese, C.; Hancock, J. M.; Xiong, Y.; Jenekhe, S. A.; Bao, Z.; Xia, Y. *Nano Lett.* **2007**, *7*, 2847–2853.
(25) De Luca, G.; Liscio, A.; Maccagnani, P.; Nolde, F.; Palermo, V.; Mullen, K.; Samori, P. *Adv. Funct. Mater.* **2007**, *17*, 3791–3798.
(26) Hernando, J.; de Witte, P. A. J.; van Dijk, E.; Korterik, J.; Nolte, R. J. M.; Rowan, A. E.; Garcia-Parajo, M. F.; van Hulst, N. F. *Angew. Chem., Int. Ed.* **2004**, *43*, 4045–4049.
(27) Palermo, V.; Otten, M. B. J.; Liscio, A.; Schwartz, E.; de Witte, P. A. J.; Castriciano, M. A.; Wienk, M. M.; Nolde, F.; De Luca, G.; Cornelissen, J.; Janssen, R. A. J.; Mullen, K.; Rowan, A. E.; Nolte, R. J. M.; Samori, P. *J. Am. Chem. Soc.* **2008**, *130*, 14605–14614.

Chart 1

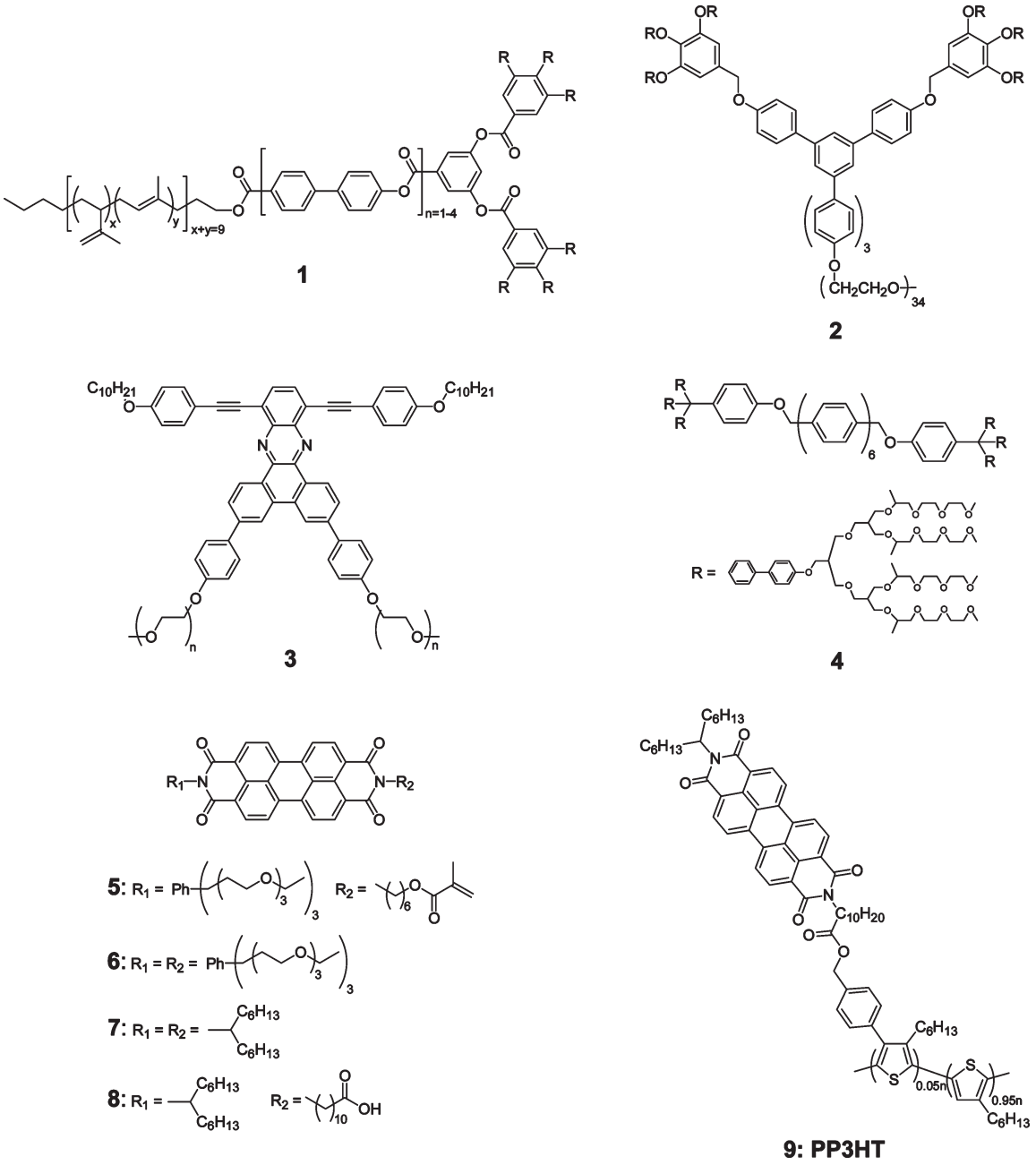

Interestingly, blends of the perylene functionalized polymer with PDI have shown that, depending on the polarity of the solvent and substrate, the two components either influence each other's morphology or self-assemble independently. Thus interplay between the polymer and PDI could be controlled by tuning the solvent or substrate polarity.[29] Alternatively, perylene diimides may be incorporated as electron-acceptors with π-conjugated polymers; such polymers have been reported wherein PDI has been incorporated as block copolymers,[30−35] in the main chain,[36] or as pendant groups.[28,37] These donor−acceptor polymers are specifically

(28) Finlayson, C. E.; Friend, R. H.; Otten, M. B. J.; Schwartz, E.; Cornelissen, J.; Nolte, R. L. M.; Rowan, A. E.; Samori, P.; Palermo, V.; Liscio, A.; Peneva, K.; Mullen, K.; Trapani, S.; Beljonne, D. *Adv. Funct. Mater.* **2008**, *18*, 3947–3955.
(29) Dabirian, R.; Palermo, V.; Liscio, A.; Schwartz, E.; Otten, M. B. J.; Finlayson, C. E.; Treossi, E.; Friend, R. H.; Calestani, G.; Mullen, K.; Nolte, R. J. M.; Rowan, A. E.; Samori, P. *J. Am. Chem. Soc.* **2009**, *131*, 7055–7063.
(30) Sommer, M.; Lindner, S. M.; Thelakkat, M. *Adv. Funct. Mater.* **2007**, *17*, 1493–1500.
(31) Lindner, S. M.; Huttner, S.; Chiche, A.; Thelakkat, M.; Krausch, G. *Angew. Chem., Int. Ed.* **2006**, *45*, 3364–3368.
(32) Sommer, M.; Lang, A. S.; Thelakkat, M. *Angew. Chem., Int. Ed.* **2008**, *47*, 7901–7904.
(33) Hua, J. L.; Meng, F. S.; Li, J.; Ding, F.; Fan, X.; Tian, H. *Eur. Polym. J.* **2006**, *42*, 2686–2694.
(34) Zhang, Q. L.; Cirpan, A.; Russell, T. P.; Emrick, T. *Macromolecules* **2009**, *42*, 1079–1082.
(35) Rajaram, S.; Armstrong, P. B.; Kim, B. J.; Frechet, J. M. J. *Chem. Mater.* **2009**, *21*, 1775–1777.
(36) Neuteboom, E. E.; Meskers, S. C. J.; van Hal, P. A.; van Duren, J. K. J.; Meijer, E. W.; Janssen, R. A. J.; Dupin, H.; Pourtois, G.; Cornil, J.; Lazzaroni, R.; Bredas, J. L.; Beljonne, D. *J. Am. Chem. Soc.* **2003**, *125*, 8625–8638.
(37) Neuteboom, E. E.; van Hal, P. A.; Janssen, R. A. J. *Chem,—Eur. J.* **2004**, *10*, 3907–3918.

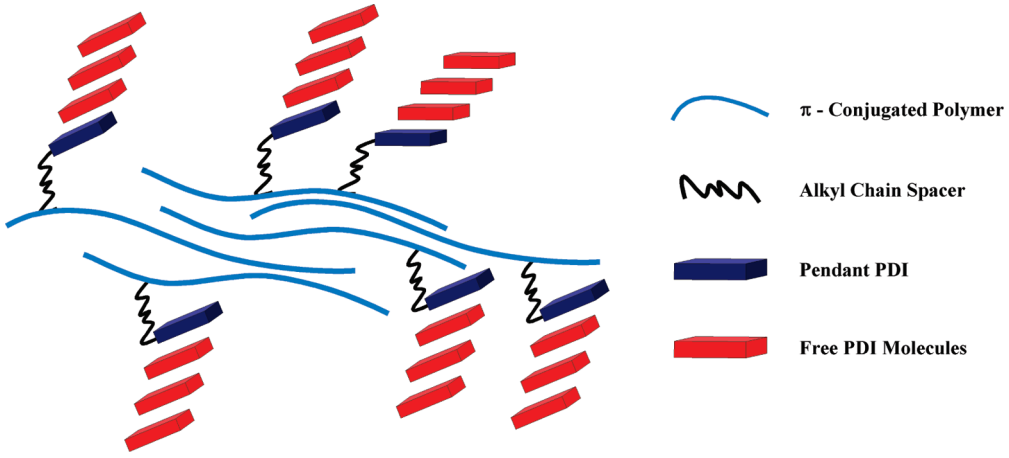

Figure 1. Schematic representation illustrating polymer-assisted crystal growth of PDI from pendant perylene moieties attached to a π-conjugated polymer.

designed to enable energy transfer in the electronically excited state of the polymer, thereby imparting useful optoelectronic properties. Furthermore, inclusion of PDI in donor−acceptor polymers results in microphase separated morphologies and photoluminescence quenching, both attractive features for photovoltaic applications.

In this work, we set to combine the formation of 1D nanowires, fabricated from PDI small molecules, with π-conjugated polymers containing pendant perylene moieties. It is hypothesized that during film formation, free PDI molecules in solution will interact with pendant perylene attached to a conjugated polymer backbone, and upon slow evaporation of solvent, molecular templating by the pendant perylene will initiate $\pi-\pi$ stacking of the PDI small molecules, as illustrated in Figure 1. In other words, polymer-assisted crystal growth of PDI may be accomplished through blending PDI small molecules with a conjugated polymer functionalized with perylene diimide. The influence of the pendant perylene moieties on the self-assembly and crystallization of PDI, and the resulting effects on thin film morphology and structure−function were investigated. This strategy involves the synthesis of a π-conjugated polymer bearing PDI side groups attached via alkyl chain spacers that allows for the rotational and translational freedom required for self-assembly. This builds on our previous work on post-functionalization of preformed poly(3-hexylthiophene) (P3HT), wherein partial bromination at the 4-position of the thienyl ring, followed by Pd-catalyzed coupling, enables the covalent attachment of a wide variety of functional groups.[38−41] Previous studies have shown that ~5 mol % postfunctionality of P3HT is optimal, i.e., 1 in 20 thienyl groups, as larger degrees of substitution disrupt the coplanarity of the π-conjugated backbone leading to reduced crystallinity in thin films.[40,42] In the present work, we report the preparation of 5 mol % postfunctionalized P3HT bearing PDI moieties (PP3HT, **9**). Comparative studies of the electronic properties of **9** by cyclic voltammetry, UV−visible and fluorescence spectroscopy using molecular blends of P3HT and PDI molecules (**7**) and blends of **9** and **7** reveal striking effects illustrating the importance of the pendant perylene moiety on the morphology and properties of the thin films formed.

Results and Discussion

Polymer Synthesis. Preparation of the desired polymer, PP3HT (**9**, Scheme 1), began with partial bromination (5 mol %, based on the number of thiophene units) via electrophilic substitution of the 4-thienyl protons of regioregular P3HT (>98% RR-P3HT). As previously reported, the extent of bromination can be monitored by ^{1}H NMR.[41] Integration of the α-methylene protons for which bromine is located on the same thienyl ring indicates that 5 mol % of the RR-P3HT backbone was brominated (**10**, see the Supporting Information, Figure S2). Suzuki cross-coupling of **10** with 4-(hydroxymethyl)phenylboronic acid following the reported method for fully functionalized P3HT afforded **11**.[43] Conversion of the bromo- to 4-(hydroxymethyl)phenyl- substituents is quantitative as evidenced by ^{1}H NMR (see the Supporting Information, Figure S3).[41]

Following a previously reported method,[44] *N,N′*-bis(1-hexylheptyl)perylene-3,4,9,10-tetracarboxylbisimide (**7**) and *N*-(1-hexylheptyl)-*N′*-(12-carboxylicdodecyl)perylene-3,4,9,10 tetracarboxylbisimide (**8**) were synthesized (see the Supporting Information for details). Briefly, condensation of perylene-3,4,9,10-tetracarboxyldianhydride with 1-hexylheptylamine afforded the symmetric diimide **7**. Partial saponification with KOH led to the monoimide monoanhydride, which following condensation with 11-aminoundecanoic acid in molten imidazole afforded **8**, a highly soluble perylene dye bearing a carboxylic acid group.

(38) Li, Y. N.; Vamvounis, G.; Holdcroft, S. *Macromolecules* **2001**, *34*, 141–143.
(39) Li, Y. N.; Vamvounis, G.; Yu, J. F.; Holdcroft, S. *Macromolecules* **2001**, *34*, 3130–3132.
(40) Li, Y. N.; Vamvounis, G.; Holdcroft, S. *Macromolecules* **2002**, *35*, 6900–6906.
(41) Zhou, Z. Y.; Chen, X. W.; Holdcroft, S. *J. Am. Chem. Soc.* **2008**, *130*, 11711–11718.
(42) Sivula, K.; Luscombe, C. K.; Thompson, B. C.; Frechet, J. M. J. *J. Am. Chem. Soc.* **2006**, *128*, 13988–13989.
(43) Chen, X. W.; Gholamkhass, B.; Han, X.; Vamvounis, G.; Holdcroft, S. *Macromol. Rapid Commun.* **2007**, *28*, 1792–1797.
(44) Holman, M. W.; Liu, R. C.; Adams, D. M. *J. Am. Chem. Soc.* **2003**, *125*, 12649–12654.

Scheme 1

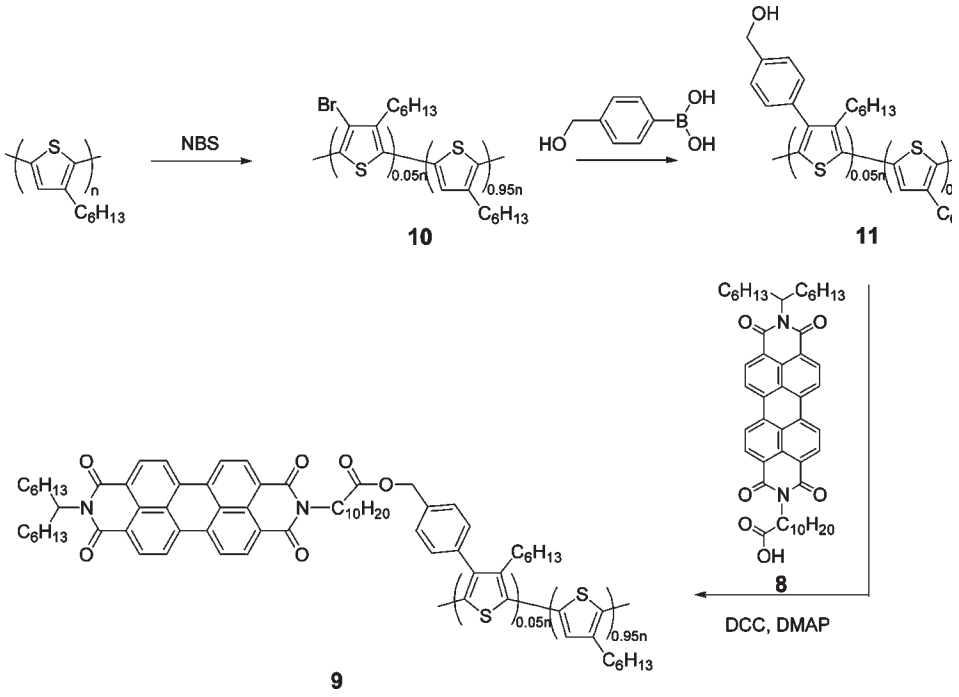

Steglich esterification of **8** and **11** afforded the desired 5 mol % postfunctionalized polymer PP3HT (**9**). Following purification, the ^{1}H NMR spectrum (see the Supporting Information, Figure S4) exhibited peaks attributable to both P3HT and perylene. The shift of the methylene peak from 4.72 ppm ($-CH_2-$OH) to 5.12 ppm ($-CH_2-$COO), which partially overlaps with the proton at 5.18 ppm ($-$NC*H*$(C_6H_{13})_2$), clearly indicates complete esterification. Furthermore, integration of the α-methylene protons of P3HT (2.78 ppm) and aromatic protons of perylene (8.68 ppm) confirms that 1 in 20 of the thienyl units was functionalized with PDI. This corresponds to a mass ratio of 4 to 1 for P3HT with respect to PDI.

Spectroscopic Properties in Solution. The optical absorption and emission spectra of dilute tetrahydrofuran (THF) solutions (5.0 mg/L) of PDI (**7**), P3HT, PP3HT (**9**), and a mixture of P3HT:PDI in a 4:1 wt ratio (corresponding to the weight ratio of PDI moieties relative to P3HT in PP3HT) were investigated. The results, illustrated in Figure 2, reveal a maximum absorption band at 445 nm and a broad emission band at 573 nm with a shoulder at 612 nm observed for P3HT. The absorption and emission spectra of PDI (**7**) exhibit three absorption peaks at 450, 485, and 520 nm and a fluorescence spectrum that is the mirror image of the absorption spectrum with peaks at 530, 570, and 620 nm.[45,46]

Solutions of PP3HT (**9**) and mixtures of P3HT:PDI (**7**) in a 4:1 wt ratio reveal almost identical absorption spectra and contain peaks corresponding to both P3HT and PDI (see Figure 2a). This similarity in absorption spectra, peak position and relative intensity, is indicative of little or no electronic interaction in the ground state between the polymer backbone in **9** and pendant perylene moieties.[26] Comparison of the photoluminescence spectra (PL), however, reveal a significant difference between solutions of PP3HT and 4:1 wt ratio mixtures of P3HT:PDI (see Figure 2b). In the latter case, the PL spectrum is a simple superposition of the PL spectra of PDI and P3HT. Conversely, the PL spectrum of PP3HT exhibits much weaker emission from both the PDI and P3HT moieties with a quantum yield of 18% (cf. 48% for 4:1 wt ratio P3HT:PDI, 68% for PDI, and 26% for P3HT).[43] PL quenching observed in solutions of PP3HT (**9**) is indicative of enhanced intramolecular interaction (namely, photoinduced electron transfer) between P3HT and PDI in the excited state, compared to solution blends of P3HT and PDI.[47,48]

Electrochemical and Spectroscopic Studies of Thin Films. The redox properties of thin films of P3HT, PDI (**7**) and PP3HT (**9**) were probed by cyclic voltammetry (CV). The results, illustrated in Figure 3, provide insight into the electronic structure of the polymers and PDI molecules as estimates of HOMO and LUMO energy levels may be calculated from the onset of redox peaks. As previously reported, thin films of P3HT show quasi-reversible oxidation and reduction waves corresponding to the formation of radical cation and radical anion species, respectively.[49] Onset potentials of +0.08 V for oxidation and −2.24 V for reduction correspond to HOMO and LUMO energy levels of 4.9 and 2.6 eV, respectively. Because of the greater electronegative

(45) Wurthner, F. *Chem. Commun*. **2004**, 1564–1579.
(46) Balakrishnan, K.; Datar, A.; Naddo, T.; Huang, J. L.; Oitker, R.; Yen, M.; Zhao, J. C.; Zang, L. *J. Am. Chem. Soc*. **2006**, *128*, 7390–7398.
(47) van Herrikhuyzen, J.; Syamakumari, A.; Schenning, A.; Meijer, E. W. *J. Am. Chem. Soc*. **2004**, *126*, 10021–10027.
(48) Wurthner, F.; Thalacker, C.; Diele, S.; Tschierske, C. *Chemistry-a European Journal* **2001**, *7*, 2245–2253.
(49) Chua, L. L.; Zaumseil, J.; Chang, J. F.; Ou, E. C. W.; Ho, P. K. H.; Sirringhaus, H.; Friend, R. H. *Nature* **2005**, *434*, 194–199.

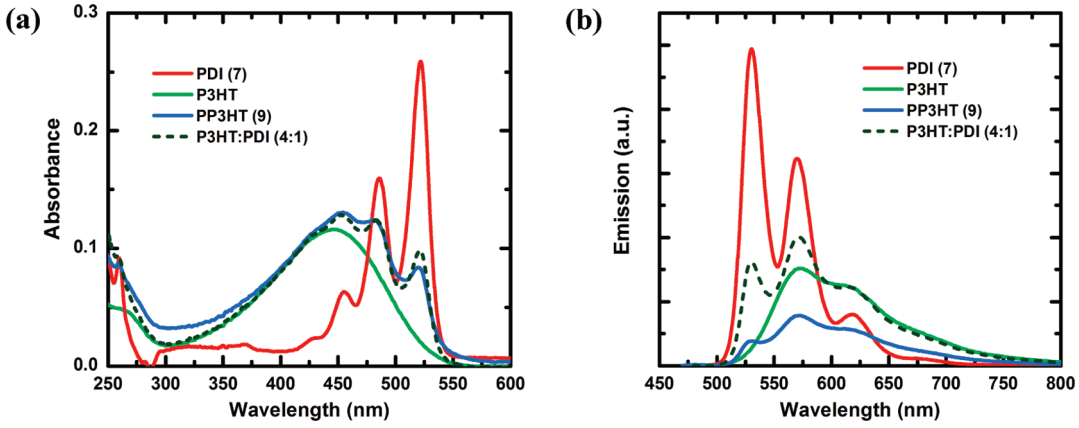

Figure 2. Optical (a) absorption and (b) emission spectra (λ_{ex} = 450 nm) of dilute THF solutions (5.0 mg/L) of PDI (**7**) (red), P3HT (green), PP3HT (**9**) (blue), and a 4:1 mixture of P3HT:PDI (dashed dark green).

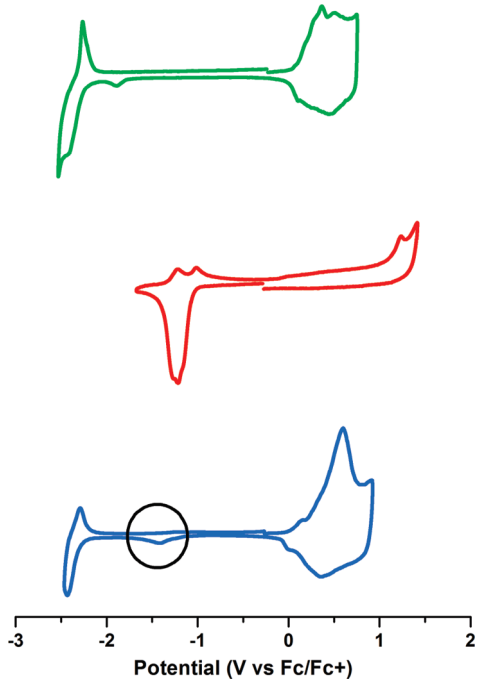

Figure 3. CV scans of thin films of P3HT (top), PDI (**7**) (middle), and PP3HT (**9**) (bottom) in acetonitrile with *n*-Bu_4NClO_4 supporting electrolyte.

character of PDI (**7**), a higher onset oxidation potential, at +1.06 V, and lower reduction potential, at −1.05 V, is observed. These potentials correspond to HOMO and LUMO levels of 5.9 and 3.7 eV, respectively. As expected, the CV of PP3HT is similar to P3HT with onset potentials of +0.08 and −2.24 V for oxidation and reduction, respectively. In contrast, however, a small reduction wave due to the presence of perylene diimide moieties was observed with an onset potential at −1.1 V (highlighted by a circle in Figure 3).

The optical properties of spin-cast thin films of PDI (**7**), P3HT, and PP3HT (**9**) as well as blends of P3HT:PDI and blends of PP3HT:PDI in 1:1, 1:2, and 1:4 wt ratios were probed by UV−vis and PL spectroscopy. All polymeric films were fabricated following the "solvent annealing" procedure previously described for P3HT:PCBM photovoltaic devices, which is reported to afford an extensively self-assembled polymer network.[50] Following spin-coating, this slow growth approach allows the film to stand in the liquid phase while the solvent slowly evaporates (see the Experimental Section for more details). Not surprisingly, the absorption spectra of the thin film blends of P3HT:PDI correspond to the direct superposition of P3HT and PDI absorption profiles for a given weight ratio (see Figure 4a). In the case of PP3HT:PDI blends, however, the absorbance at 495 nm remains constant while the peak at 530 nm increases as the concentration of PDI increases. Furthermore, the intensity of the shoulder observed at 597 nm decreases with increasing PDI content, indicative of weakening of the intermolecular interchain interactions within the π-conjugated polymer.[51] In fact, for a 1:4 wt ratio blend, the shoulder is no longer present. This may be attributed to increased twisting of the PP3HT polymer backbone or the result of packing phenomenon associated with increasing PDI content as indicated by thin film morphological studies, which reveal 1D nanostructures of the perylene molecules (see section on thin film morphology).

Quantum yields of PL (Φ_{PL}), reported in Table 1, exemplify the fluorescence quenching observed in blends of P3HT:PDI and PP3HT:PDI. Because the Φ_{PL} for PDI is larger than P3HT and PP3HT, increasing PDI content in thin film blends with both P3HT and PP3HT should increase the fluorescence quantum yields if there is little to no molecular interaction between the conjugated polymers and PDI. In blends of P3HT:PDI, the decrease in PL intensity with decreasing PDI content is gradual and is attributed mostly to a lowering of the relative PDI content in the films rather than to quenching from interaction between the PDI molecules and the polymer. On the other hand, thin film blends of PP3HT:PDI exhibit a significantly greater effect of the polymer on the PL intensity (see Figure 5 and the Supporting Information, Figure S5). For example, comparison of the PL spectra of 1:4 wt ratio blends of PP3HT:PDI and P3HT:PDI show that

(50) Li, G.; Yao, Y.; Yang, H.; Shrotriya, V.; Yang, G.; Yang, Y. *Adv. Funct. Mater.* **2007**, *17*, 1636–1644.
(51) Dittmer, J. J.; Marseglia, E. A.; Friend, R. H. *Adv. Mater.* **2000**, *12*, 1270–1274.

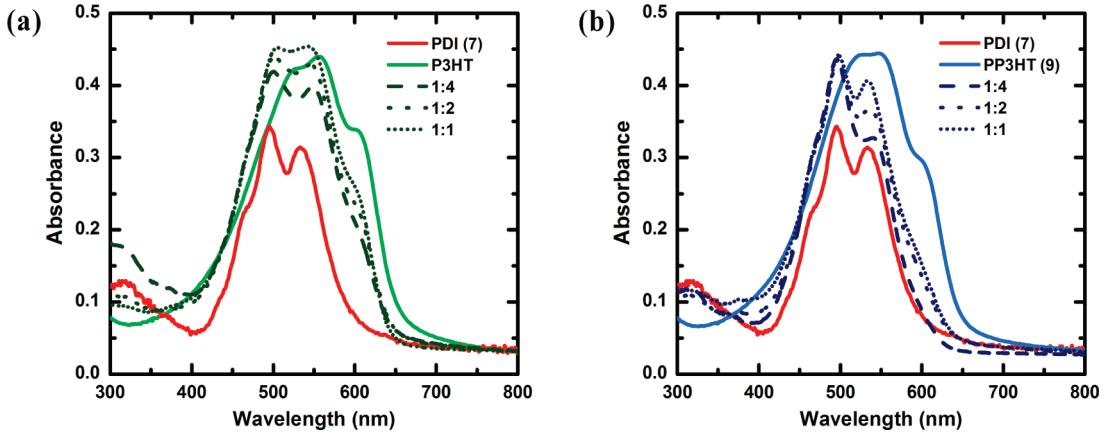

Figure 4. Optical absorption spectra of thin films of (a) P3HT (green), PDI (7) (red), and blends of P3HT:PDI (dark green) in 1:1, 1:2, and 1:4 wt ratios and (b) PP3HT (**9**) (blue), PDI (**7**) (red), and blends of PP3HT:PDI (navy) in 1:1, 1:2, and 1:4 wt ratios.

Table 1. Thin film PL quantum yields for pristine films and blends of P3HT and PP3HT with PDI for various weight ratios

				P3HT:PDI			PP3HT:PDI		
Blend	**P3HT**[a]	**PP3HT**[a]	**PDI**[a]	**1:1**[b]	**1:2**[a]	**1:4**[a]	**1:1**[b]	**1:2**[b]	**1:4**[a]
Φ (%)	1.9	0.5	5.5	0.3	0.5	2.1	0.07	0.2	0.3

[a] Quantum yield measured directly by integrating sphere (λ_{ex} = 500 nm). [b] Quantum yield calculated using the following equation $\Phi_u = \Phi_{PDI}(I_u/I_{PDI})(A_{PDI}/A_u)$, where subscripts u and PDI refer to the unknown and perylene, respectively; A corresponds to the optical density at the excitation wavelength (λ_{ex} = 500 nm); I is the integrated emission.

fluorescence is quenched to a much greater extent in the PP3HT:PDI blends, e.g., quantum yields for 1:4 blends of PP3HT:PDI and P3HT:PDI are 0.3% vs 2.1%, respectively. Increased quenching provides further evidence of increased interaction between the conjugated polymer and PDI but may also be indicative of long-range order (e.g., 1D nanostructure) of perylene molecules as fluorescence quenching is typically indicative of $\pi-\pi$ stacking due to the forbidden low-energy excitonic transition.[52]

Thin Film Morphology. The thin film morphology of P3HT, PP3HT and their blends with PDI were examined by transmission electron microscopy (TEM). All polymeric films were fabricated following the "solvent annealing" procedure described previously (see Experimental Section for more details).[50] To investigate phase separation, films were stained with RuO_4, which preferentially stains the P3HT domains, producing highly scattering RuO_2.[53] The micrographs, shown in Figure 6, show light and dark areas representing regions of PDI and P3HT, respectively. The TEM images reveal that films of PP3HT exhibit a feathered lamella pattern with phase segregated domains of ~20 nm. When blended with PDI in a 1:1 wt ratio, intriguing 1D assemblies of PDI are observed uniformly distributed within the film, ~200 nm wide and several micrometers in length. Increasing the PDI content by preparing a 1:2 wt ratio PP3HT:PDI film enhances the connectivity and continuity of the network of 1D PDI. As a control experiment, the morphology of P3HT blended with PDI was investigated. As confirmed by TEM of the 1:1 and 1:2 wt blends of P3HT:PDI, shown in Figure 6, no 1D assemblies were observed, but rather, microphase segregated morphologies. This clearly illustrates that 1D self-assemblies of PDI are templated by the perylene molecule attached to P3HT and not simply by the P3HT backbone.

TEM images of the regions in-between the PDI nanowires formed in PP3HT:PDI blends are shown in images c and d in Figure 6. The images indicate that phase segregation of the conjugated polymer and PDI also exists, but the length scale is much smaller and dependent on the PDI content, i.e., an increase in PDI content from 1:1 to 1:2 results in a decrease in domain size from 8 to 4 nm, respectively. In stark contrast, blends of P3HT and PDI form random, micrometer-sized crystallites (Figure 6e, 6f). PDI alone forms polycrystalline films comprising 50 nm crystallites (Figure 6h).

To further explore the influence of the pendant perylene moieties in PP3HT on the molecular assembly of PDI in thin film blends, we obtained TEM images of the cross-sectioned films. A micrograph of PP3HT:PDI with 1:2 wt ratio, shown in Figure 7, reveals anisotropic, 10−20 nm thick, linear assemblies of PDI running parallel to the surface of the substrate. If the linear arrangement of PDI is driven by $\pi-\pi$ interactions, then one may assume PDI π-stacks are formed and, depending on the orientation of the pendant PDI, these π-stacks may arrange perpendicular to the surface of the substrate. Alternatively, the pendant PDI molecules may arrange perpendicular to the polymer chain thus forming π-stacked columns of PDI running parallel to the substrate surface (see Figure 7c). In contrast, blends of P3HT:PDI (1:2 wt ratio) form agglomerates (or nanocrystals) of PDI molecules randomly distributed throughout the film, as opposed to linear assemblies. The schematic representation in Figure 7 is provided to illustrate the difference in thin film morphologies when PDI is blended with PP3HT and P3HT.

Thin Film X-ray Diffraction. X-ray diffraction (XRD) experiments were carried out to probe the molecular

(52) Balakrishnan, K.; Datar, A.; Oitker, R.; Chen, H.; Zuo, J. M.; Zang, L. *J. Am. Chem. Soc.* **2005**, *127*, 10496–10497.
(53) Trent, J. S.; Scheinbeim, J. I.; Couchman, P. R. *Macromolecules* **1983**, *16*, 589–598.

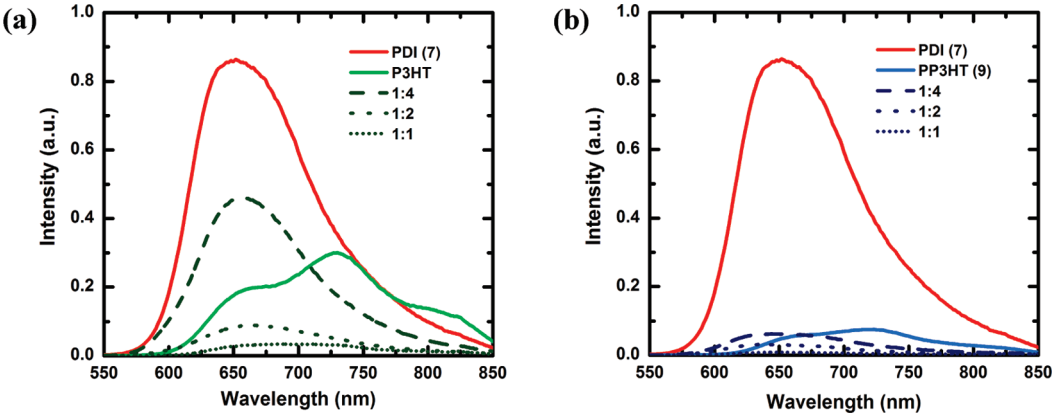

Figure 5. Emission spectra (λ_{ex} = 500 nm) of thin films of (a) P3HT (green), PDI (7) (red), and blends of P3HT:PDI (dark green) in 1:1, 1:2, and 1:4 wt ratios and (b) PP3HT (**9**) (blue), PDI (**7**) (red), and blends of PP3HT:PDI (navy) in 1:1, 1:2, and 1:4 wt ratios. The spectra are corrected for the optical density at the excitation wavelength.

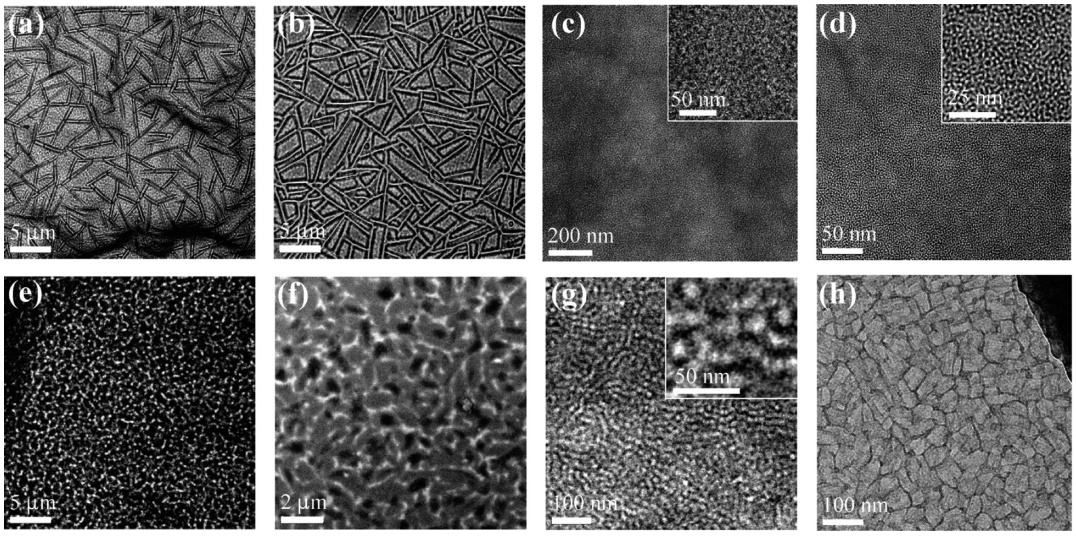

Figure 6. Transmission electron micrographs for thin films of PP3HT:PDI for (a, c) 1:1 and (b, d) 1:2 wt ratios; (c, d) higher magnification of the interstitial regions. For comparative purposes, TEM micrographs of P3HT:PDI of (e) 1:1 and (f) 1:2 wt ratio films, and pristine films of (g) PP3HT and (h) PDI are also shown.

arrangement of free PDI molecules in the films. The XRD patterns (see the Supporting Information, Figure S6) for thin films of P3HT and PP3HT exhibit first-order reflections at 2θ angles of 5.49° and 5.33°, respectively. The lower diffraction angle observed for PP3HT, compared with P3HT, is indicative of an increased interlamellar spacing as would be expected upon attachment of pendant PDI. In addition to a peak at 4.52°, the XRD pattern for PDI shows clearly resolved peaks corresponding to first, second, third, and fourth order reflections at 2θ angles of 5.01°, 9.99°, 15.0° and 20.04°, respectively. The first and second diffraction peak (with *d*-spacing of 19.53 and 17.6 Å, respectively) are assigned to the edge-to-edge distances between two adjacent PDI molecules. For comparative purposes, XRD experiments were performed on thin film blends of P3HT:PDI in 4:1 and 1:2 wt ratios. Introduction of PDI into a film of P3HT in a 4:1 wt ratio (corresponding to the wt ratio of P3HT:PDI in PP3HT) results in a broad peak between 4.0°−5.9° with two sharp peaks at 2θ angles of 4.425° and 5.37°. Interestingly, the peak at 5.37° is similar to the diffraction peak observed in thin films of PP3HT (*cf.* 5.49° for P3HT films) and the peak at 4.425° is observed at very low intensity in pristine films of PDI. Increasing the PDI content, as in the 1:2 P3HT:PDI wt ratio blends, yields a sharp diffraction peak at 5.01° on top of a broad diffraction from 4.0°−5.9°.

Introduction of PDI into thin film blends with PP3HT, as in the case for 1:1 wt ratio blends, results in a decrease in crystallinity within the PP3HT film (as evidenced by broadening of the diffraction peak from 3.8°−5.7°). There is, however, a sharp diffraction peak at 4.99° corresponding to ordering of PDI within the blend. Further increasing the PDI content (as in the 1:2 PP3HT:PDI wt ratio blends) increases the degree of crystallinity of PDI as evidenced by the sharp diffraction peaks at 5.01° and 7.71°. The peak at 5.01° corresponds to packing of PDI; however, the new peak observed at 7.71° may be due to interaction between the free PDI molecules and the pendant PDI moieties. The XRD data are consistent with the morphologies observed by TEM upon increasing the PDI content, i.e., the content of crystalline PDI in the film is increased.

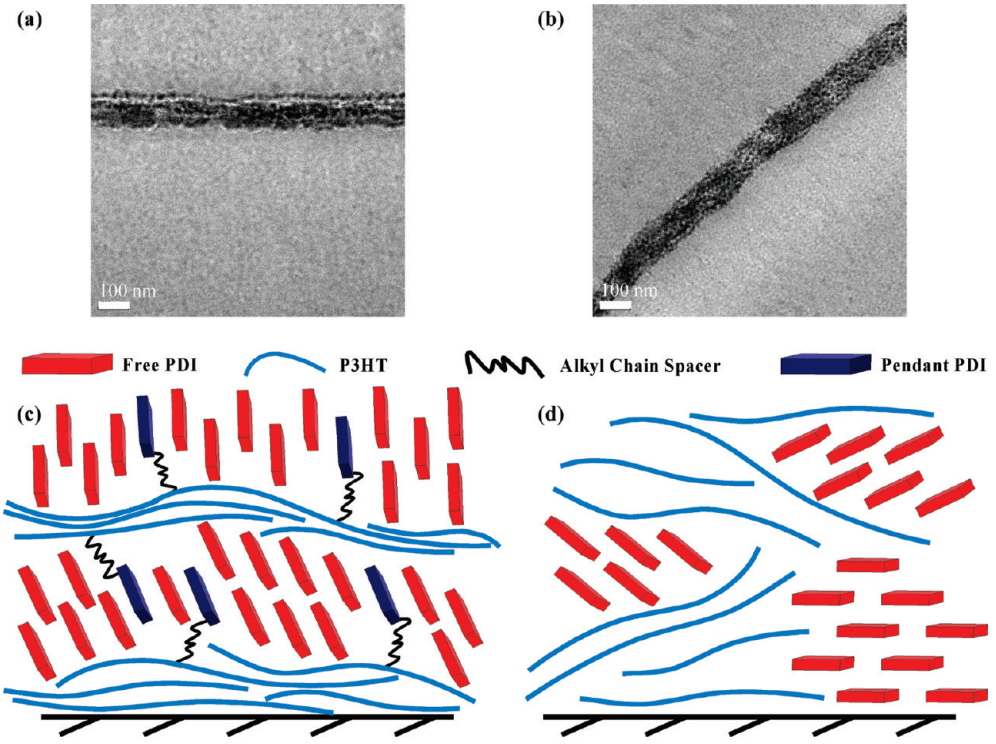

Figure 7. Top panel, cross-sectional transmission electron micrographs for thin film blends of (a) PP3HT:PDI and (b) P3HT:PDI in 1:2 wt ratio. Bottom panel, schematic representation illustrating the morphological effect of pendant PDI in PP3HT on (c) blends with free PDI compared with (d) blends of P3HT:PDI.

If the PDI molecules are linearly arranged due to $\pi-\pi$ interactions, the XRD pattern should exhibit peaks corresponding to a *d*-spacing of <5.0 Å (because $\pi-\pi$ interactions of $\sim$3.3−3.6 Å typically correspond to repeat units of <5 Å).[45,54] Unfortunately, inspection of the XRD patterns obtained for blends of PP3HT:PDI in 1:1 and 1:2 wt ratios did not reveal peaks corresponding to $\pi-\pi$ interactions. The absence of these diffraction peaks, however, does not strictly imply that $\pi-\pi$ interactions are absent, as the films are thin (100 nm) and TEM images reveal the 1D assemblies to be only 10−20 nm thick. Furthermore, XRD measurements were obtained using glass substrates that inherently yield a broad diffraction peak in the region where $\pi-\pi$ interactions would be observed.

Summary and Conclusions

In this work, we report a chemical strategy to form 1D nanoarchitectures of PDI within a conjugated polymer. The anisotropy of these organized PDI structures is confirmed by cross-sectional TEM, which show the 1D assemblies aligning parallel to the substrate surface. This work therefore provides evidence of polymer-assisted crystal growth of perylene diimide in which the polymer itself is an optoelectronically active material. The origin of these unique morphologies lies in the difference in solubility of the conjugated polymer and the PDI. The conjugated polymer, being less soluble, nucleates from the casting solution as solvent evaporates−incorporating a fraction of PDI because of the attachment of PDI to the polymer backbone. During the process of polymer deposition, the crystallization of free PDI by the polymer is templated parallel to the substrate's surface.

Surrounding the 1D structures of PDI is a heterogeneous PP3HT:PDI blend. The size domain of the polymeric component is substantially reduced in the presence of PDI when compared to pristine PP3HT films. This therefore indicates that the presence of PDI restricts long-range organization of the conjugated polymer. In fact, the crystalline domains of the polymer cannot be observed in these blends by XRD as is common for P3HT polymers, although the absorption spectra of PP3HT and its blends are consistent with a highly organized structure. Indeed, excitation energy in thin film blends of PP3HT:PDI is quenched to a much greater extent than direct blends of P3HT and PDI, which is indicative of enhanced electron transfer between the donor and acceptor species. Thus, at one level, nanosized domains of π-conjugated polymer are in intimate contact with PDI domains (in the sub-10 nm range), but at a higher level micrometer-scale crystallites of PDI domains phase segregate from the conjugated polymer. Studies aimed at investigating these blends as active layers in photovoltaic devices are currently underway, as are further investigations into the stacking orientation of PDI molecules within the 1D arrays. Moreover, the effect of side chain substitution of the PDI molecules on the thin film morphology in PP3HT blends may lead to innovative supramolecular structures that may be tailored for optoelectronic applications.

Experimental Section

General Procedures. ^{1}H spectra were obtained on a 500 MHz Varian AS500 spectrometer; chemical shifts are reported in

(54) Klebe, G.; Graser, F.; Hadicke, E.; Berndt, J. *Acta Crystallogr., Sect. B* **1989**, *45*, 69–77.

parts per million (ppm), referenced to $CDCl_3$ (^1H: $\delta = 7.26$). Molecular weights were measured by gel permeation chromatography (GPC) (Waters model 1515 isocratic pump) equipped with μ-Styragel columns against polystyrene standards. Polymers were eluted with THF using a flow rate of 1.0 mL/min and detected with a UV−vis detector (Waters model 2487) at 254 nm. Elemental analyses were obtained using a Carlo Erba model 1106 CHN analyzer. UV−vis absorption spectra were recorded on a Cary 3EI (Varian) spectrophotometer. Photoluminescence (PL) spectra were recorded with a Photon Technology International QuantumMaster model QM-4 equipped with an integrating sphere. Film thickness and surface roughness were measured on a KLA-Tencor Alpha-Step IQ Surface Profiler.

Electrochemistry. Cyclic voltammetry was performed on a Princeton Applied Research Model 263A potentiostat/galvanostat in a one compartment, three-electrode cell in acetonitrile (ACN) solution of 0.1 M *n*-Bu_4NClO_4 at a scan rates of 50 mV s^{-1}. A glassy-carbon disk coated with polymer and Pt wire were used as the working and counter electrodes, respectively, and a Pt wire in an ACN solution of 0.1 M Bu_4NI/ 0.05 M I_2, separated from the working electrode compartment by a glassy frit, was used as the reference electrode. An internal reference to ferrocene (Fc/Fc^+ redox couple is 4.8 eV) was used to calibrate the reference electrode.

Fabrication of Polymer Thin Films. Polymeric films were fabricated following the "solvent annealing" procedure described by Li et al.[50] Dichorobenzene solutions (20 mg/mL) of PP3HT, P3HT, PDI and blends of PP3HT:PDI and P3HT:PDI at various weight ratios were spin-coated at 100 rpm for 1 s, 300 rpm for 1 s and 900 rpm for 20 s onto PEDOT coated glass substrates in a glovebox under N_2-filled atmosphere. Following spin-coating, the substrates were left in a covered glass Petri dish for one hour to allow for slow evaporation of the solvent, resulting in 70−80 nm thick films as measured by profilometry.

Transmission Electron Microscopy. TEM images were performed on a Tecnai 20 FEI STEM. A layer of poly(styrene sulfonic acid)-doped poly(3, 4-ethylenedioxythiophene) (PEDOT, BaytonP VP AI4083) was spin-cast onto clean glass substrates at 5000 rpm then annealed at 140 °C for 10 min. Onto this surface, polymers and polymer blends were fabricated following the "solvent annealing" procedure described above. The film and substrate were immersed in water, and upon dissolution of the PEDOT layer, the polymer films were removed from the surface of the water using Cu grids. The films were then stained for 15 min using of RuO_4 vapor prepared in situ from 0.5% ruthenium(III) chloride in a sodium hypochlorite solution (containing ≥4% chlorine in solution).

X-ray Measurements. XRD was performed on a Bruker-AXS D8 Discover High-Resolution Diffractometer system using Cu Ka wavelength (about 1.544 Å). Polymer films were prepared on glass substrates by the same spin casting method described before.

Acknowledgment. We are grateful to the Natural Sciences and Engineering Research Council of Canada (NSERC) for financial support and for an NSERC postdoctoral fellowship to JLB The authors also thank Dr. Xiwen Chen (SFU) and Bobak Gholamkhass (SFU) for useful discussions.

Supporting Information Available: Experimental details; ^1H NMR for compounds **10**, **11**, PP3HT (**9**), and RR-P3HT; thin film emission spectra for RR-P3HT, PP3HT, and blends of P3HT:PDI and PP3HT:PDI in 1:1, 1:2, and 1:4 wt ratios; thin film XRD patterns for PDI, P3HT, PP3HT, blends of P3HT:PDI in 1:2 and 4:1 wt ratios, and blends of PP3HT:PDI in 1:1 and 1:2 wt ratios (PDF). This material is available free of charge via the Internet at http://pubs.acs.org.